Liquid Crystals
Publication details, including instructions for authors and subscription information:
http://www.informaworld.com/smpp/title~content=t713926090

Cholesteric helix: topological problem, photonics and electro-optics

Lev M. Blinov[ab]; Serguei P. Palto[b]
[a] Shubnikov Institute of Crystallography RAS, Moscow, Russia [b] Physics Department, Calabria University, Rende, Italy

First published on: 10 July 2009

To cite this Article Blinov, Lev M. and Palto, Serguei P.(2009) 'Cholesteric helix: topological problem, photonics and electro-optics', Liquid Crystals, 36: 10, 1037 — 1047, First published on: 10 July 2009 (iFirst)
To link to this Article: DOI: 10.1080/02678290902761356
URL: http://dx.doi.org/10.1080/02678290902761356

Liquid Crystals,
Vol. 36, Nos. 10–11, October–November 2009, 1037–1047

Taylor & Francis
Taylor & Francis Group

INVITED ARTICLE

Cholesteric helix: topological problem, photonics and electro-optics

Lev M. Blinov[a,b]* and Serguei P. Palto[b]

[a]*Shubnikov Institute of Crystallography RAS, 119333, Leninsky Prospect 59, Moscow, Russia;* [b]*Physics Department, Calabria University, Rende, 87046, Italy*

(Received 10 December 2008; final form 19 January 2009)

Using numerical simulations and the results of our experiments we discuss the behaviour of a defect-free cholesteric liquid crystal in rather a strong electric field. The smooth helix unwinding predicted by de Gennes (*Solid State Commun.* **1968**, *6*, 163,) occurs under the thermodynamic equilibrium conditions and can easily proceed with the assistance of multiple defects. The defect-free helix in the field strictly perpendicular to the helical axis cannot be unwound for topological reasons. The field deforms the helix without a change of its period and induces higher harmonics of the helical structure. Due to the latter, the shape of the Bragg photonic stop-band changes and a second-order photonic band is observed in the optical transmission. Moreover, novel laser effects are predicted by modelling for the dye-doped, distorted cholesteric structure. The same field-induced anharmonicity results in a strong change of the polarisation state of the beam passing the helical structure along its axis. Due to fast relaxation of the higher harmonics, the switching time of the devices using the corresponding electro-optical effect (called in-plane switching) can be improved significantly. This is shown both experimentally and by numerical calculations.

Keywords: liquid crystals; laser; electro-optics

1. Introduction

The influence of the works of the Orsay Liquid Crystal Group on the development of the physics of liquid crystals all over the world is enormous. In the epicentre of the vigorous activity of the group, especially in late 1960s and 1970s, was the giant figure of P.G. de Gennes. His personal contribution in just two years (1968–69) is unbelievable; see (*1*): the prediction of the transition from cholesteric to nematic structure (*1a*); description of the director fluctuations in nematics, both static (*1b*) and dynamic (*1c*); development of the phenomenological theory of isotropic liquid – nematic phase transition (*1d*); formulation of basic equations for SmA elasticity and description of the flexoelectric effect in the SmA phase (*1e*). All of these papers became classical.

Both present authors have had the pleasure of working in the Orsay laboratory with the people from the famous group for, regrettably, a quite short period. The older of us was acquainted with Pierre Gilles and for all of his life was under the strong influence of his scientific and artistic talent. So we are happy to present this paper as our modest contribution to the memorial book. In this paper, we will present some new data and ideas related to one of the seminal articles written by P.G. de Gennes at the beginning of his fruitful work in the field of liquid crystals (*1a*).

The plan of the paper is as follows. First, we recap on the essence of the cholesteric helix unwinding effect. Then we discuss some limitations of the thermodynamic approach when we deal with a defect-free helix in the field perpendicular to the helical axis. We show some experimental results and corresponding modelling. Next, we examine optical transmission of and lasing in the field-distorted helix in terms of the higher-order photonic stop-bands. The simulation results may be useful for lasers and other photonic devices. Finally, we describe a new electro-optical effect based on the field induced anharmonicity in a helical structure that shows a high contrast and short switching times, down to the microsecond range, suitable for fast light modulators and displays.

2. Untwisting of the cholesteric helix

2.1 de Gennes model

de Gennes (*1a*) has considered an unlimited cholesteric with a helix axis ($h \| z$) in magnetic field H perpendicular to h (Figure 1(a)). The magnetic anisotropy is positive $\chi_a = \chi_{\|} - \chi_{\perp} > 0$. The critical field for the helix unwinding can be calculated from the difference between the free energy density of the cholesteric and nematic structures, which is:

$$\begin{aligned}\Delta g = g_{Ch} - g_N &= \frac{1}{2}\left[K_{22}\left(\frac{d\phi}{dz} - q_0\right)^2 - \chi_a H^2 \cos^2\phi\right] \\ &\quad - \frac{1}{2}\left[K_{22}(-q_0)^2 - \chi_a H^2\right] \\ &= \frac{1}{2}K_{22}\left[\left(\frac{d\phi}{dz}\right)^2 - 2q_0\frac{d\phi}{dz}\right] + \frac{1}{2}\chi_a H^2 \sin^2\phi, \qquad (1)\end{aligned}$$

*Corresponding author. Email: lev39blinov@gmail.com

ISSN 0267-8292 print/ISSN 1366-5855 online

DOI: 10.1080/02678290902761356
http://www.informaworld.com

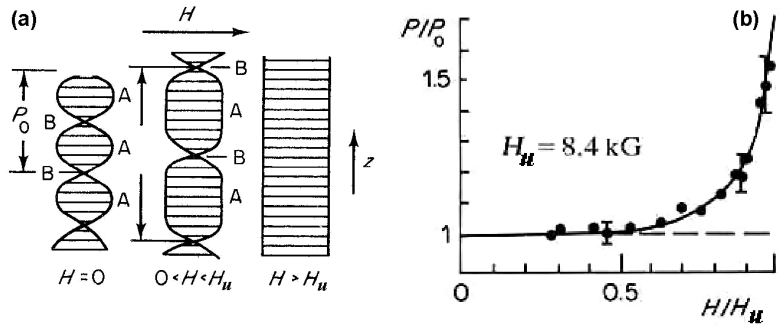

Figure 1. (a) de Gennes model. Influence of a magnetic field **H** on the planar cholesteric texture having $\chi_a > 0$. The helical axis is parallel to z. Horizontal lines show the projections of the director onto **H**. (b) Dependence of helix pitch ratio (P/P_0) on the normalised magnetic field strength with the de Gennes theoretical curve superimposed on the experimental points (PAA, $d = 130$ μm, $P_0 = 13$ μm, $H_u = 8.4$ kG (2)).

where $q_0 = 2\pi/P_0$ corresponds to a wavevector of the helical distribution with a pitch of P_0, and φ is the twist angle describing the helical distribution of the director in the field-off state. It also equals an angle between the director and the field. Note that, for an unwound cholesteric, $\partial\varphi/\partial z = 0$, $\varphi = 0$ or π. Introducing the field coherence length ξ ($\xi^2 = K_{22}/\chi_a H^2$) and integrating over one period of the helix P_0 along the z-axis we get:

$$\frac{\Delta G}{\chi_a H^2} = \frac{1}{\chi_a H^2}\int_0^{P_0} \Delta g dz = \int_0^{P_0}\left[\frac{1}{2}\xi^2\left(\frac{d\phi}{dz}\right)^2 - q_0\xi^2\frac{d\phi}{dz} + \frac{1}{2}\sin^2\phi\right]dz \quad (2)$$

where ΔG is the difference in total free energy attributed to a volume on a scale of pitch P_0.

The Euler–Lagrange equation corresponding to the free energy density of the cholesteric structure reads:

$$\xi^2\frac{d^2\phi}{dz^2} = \sin\phi\cos\phi \text{ or } \frac{1}{2}\xi^2\frac{d}{dz}\left(\frac{d\phi}{dz}\right)^2 = \sin\phi\cos\phi\frac{d\phi}{dz}. \quad (3)$$

Equation (3) is easily integrated:

$$\xi^2\left(\frac{d\phi}{dz}\right)^2 = 2\int_z \sin\phi\cos\phi\frac{d\phi}{dz}dz = 2\int_\phi \sin\phi\cos\phi d\phi = \sin^2\phi + C. \quad (4)$$

For the particular periodic structure shown in Figure 1(a), the derivative $d\varphi/dz = 0$ at any z where $\varphi = 0$ or π (middle points in regions A). Therefore, $C = 0$ and $\xi(d\varphi/dz) = \pm\sin\varphi$, where for a right-handed helix the sign at the right site is either positive (if φ belongs to an interval from 0 to π) or negative (if $\pi < \varphi < 2\pi$). Then, substituting Equation (4) into Equation (2) we find:

$$\frac{\Delta G}{\chi_a H^2} = \int_0^{P_0}\xi^2\left[\left(\frac{d\phi}{dz}\right)^2 - q_0\frac{d\phi}{dz}\right]dz = \xi^2\int_0^{2\pi}\left(\frac{d\phi}{dz} - q_0\right)d\phi = 2\xi\int_0^{\pi}\sin\phi\, d\phi - q_0\xi^2\int_0^{2\pi}d\phi = 2\xi(2 - \pi q_0\xi). \quad (5)$$

Therefore the threshold condition ($\Delta G = 0$) for the helix unwinding or the *cholesteric nematic transition* reads

$$\xi_u = \frac{2}{\pi q_0} \text{ or } H_u = \frac{\pi^2}{P_0}\sqrt{\frac{K_{22}}{\chi_a}}. \quad (6)$$

Moreover, for $H < H_u$, de Gennes has estimated *stationary values* of the pitch and predicted its monotonic increase with increasing field:

$$P(H) = P_0\left[1 + \frac{\chi_a^2 P_0^2}{32(2\pi)^4 K_{22}^2}H^4 + \cdots\right] \quad (7)$$

The resulting Equation (6) and Equation (7) are in very good agreement with experiments fulfilled under thermodynamic equilibrium. Figure 1(b) shows the results obtained by R.B. Meyer (*2*) on rather a thick cell ($d = 130$ μm) filled with a cholesteric mixture based on *p*-azoxyanisol (PAA). The mixture was not

oriented by boundaries and contained a number of defects. Meyer mentioned that, in order to reach the equilibrium state for each value of magnetic field, 'the tendency to hysteresis was overcome by cycling the field while observing the cell'. This comment is very important because the hysteresis is a fingerprint of the topological constraints and observed many times, see e.g. (*3*). We shall come to these constraints below. In another experiment (*4*), the smooth, hysteresis-free unwinding of the helix was observed in the wedge-shaped cells with the well-known Grandjean disclinations. However, if we deal with a sample free of any defects and, in addition, with the field exactly perpendicular to the helical axis, a step-like transition to the uniform state occurs *even in the unlimited samples*.

For the electric field, in Equations (6) and (7) we should substitute χ_a with $\varepsilon_a/4\pi$. Therefore, if we apply an electric field (more convenient for practical purposes) to a real cholesteric sample for a sufficiently long time, eventually we would expect the helical pitch of the sample to change according to Equation (7). Such a field-induced pitch tuning would be very promising for application to displays, tunable photonic filters, diffraction gratings and lasers. Unfortunately, pitch tuning may be realised only via an intermediate, very slow stage of the defect formation.

2.2 *Topological limitation*

What is the reason for such a disappointing situation with tuning? It is very simple: despite the fact that field unwinding of the cholesteric helix is thermodynamically profitable there is a strong topological limitation on a smooth (continuous) unwinding process. This can be easily understood. In a zero electric field E, see Figure 2(a), we again have a helical structure of the director **n** (shown by arrows) with vertical helical axis **h**. We assume that the helix is either infinite or limited by two boundaries with infinitely weak azimuthal anchoring at least at one of the boundaries. It means that there is no confinement, which would prevent a free rotation of the non-anchored director at that boundary. Therefore unwinding the helix due to, for instance, a heating process *is possible* (*5*). Now, imagine that we apply an electric field $\mathbf{E}\perp\mathbf{h}$ to structure (a) with the aim of increasing the pitch twice, $P_E = 2P_0$, as shown in Figure 2(b). To do this we must turn the director from the central position A' with $\mathbf{n}\|\mathbf{E}$ (favourable due to $\varepsilon_a > 0$) to unfavourable position B, where $\mathbf{n}\perp\mathbf{E}$, and this situation repeats in each period. Moreover, **n** must make a *full turn against the field* on transition from the initial position A (at the bottom) to new position A'. Therefore, a very serious topological problem exists for the ideal cholesteric. In reality, the structure shown in Figure 2(c) forms with favourable orientation of the director everywhere except for the walls. The positions of the walls, W, separating areas where **n** differs by π are fixed and the energy of the structure (*c*) with the conserved pitch P_0 is, of course, larger than the most profitable stationary structure with an enhanced pitch calculated by de Gennes.

The scenario described has been confirmed by both experiment and numerical modelling (*6*). For the latter, the software used was developed earlier (*7*, *8*). For experiments, a cell, shown in Figure 3, was designed with electric voltage applied between the in-plane interdigitated electrodes separated by a distance of 20 μm. The dielectric anisotropy of the cholesteric was $\varepsilon_a = +7.8$. The same cell structure and material parameters were assumed in modelling.

In calculations, both the zenithal and azimuthal anchoring strength at the bottom substrate is strong, $W_{z1} = W_{a1} = 0.1$ mJ/m^2. At the upper substrate the

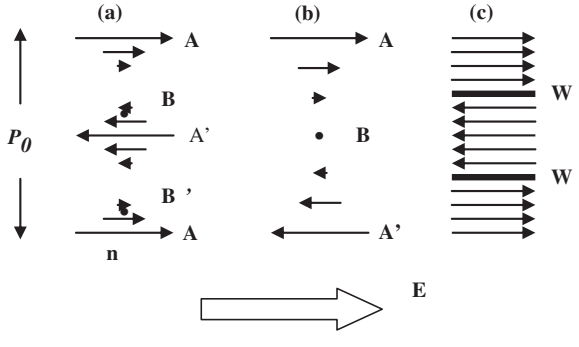

Figure 2. Non-equilibrium field behaviour of a cholesteric helix ($\varepsilon_a > 0$). (a) Zero-field structure. (b) Unfavourable structure with a hypothetical pitch $P_E = 2P_0$. (c) Favourable wall structure with unchanged pitch and multiple walls.

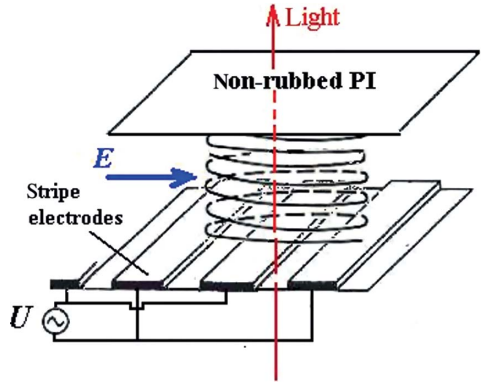

Figure 3. Helical structure of a cholesteric liquid crystal between two glass plates. On the bottom plate, an array of metal interdigitated electrodes is deposited.

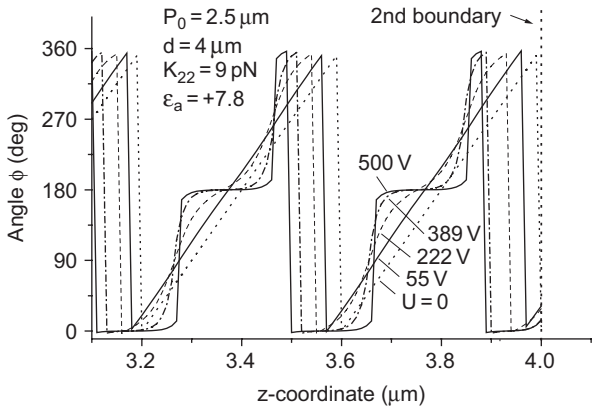

Figure 4. Director azimuth φ for the last two periods of the helix adjacent to the top boundary. It repeatedly increases from 0 ° to 360° within each period P_0.

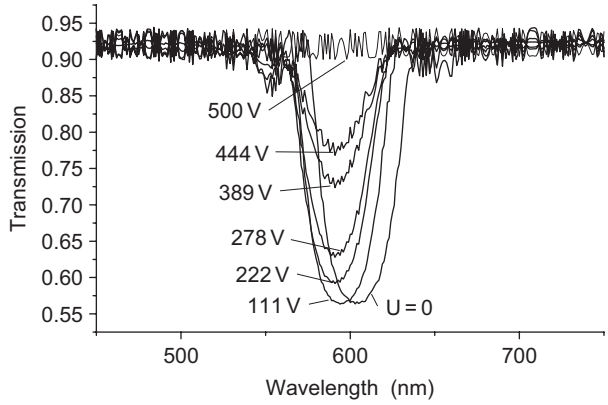

Figure 5. Calculated optical transmission spectra of the planar cholesteric texture as functions of the electric voltage applied (unpolarised light).

zenithal anchoring energy W_{z2} is also that strong, therefore the director is always confined within the plane of substrates perpendicular to the helical axis. However, the azimuthal anchoring energy at the second substrate is negligibly small, W_{a2}=0.001 mJ m^{-2}, *and provides conditions for easy sliding of the director* at the substrate surface. Figure 4 shows the calculated distribution of the azimuthal angle φ for the planar cholesteric structure of thickness $d = 25P_0$ with P_0 = 0.25 μm (only two periods are shown for clarity). Without field the azimuth linearly increases from 0° to 360° within each period P_0. With increasing voltage the dependence $\varphi(z)$ becomes strongly non-linear due to distortion of the helix, but the period of the structure remains almost unchanged. Only a small overall shift of the curves along the z-coordinate appears due to weak (few degrees) sliding of the director at the top boundary. This shift results in some decrease of the helix pitch, but this decrease cannot exceed a value of $P_0/4N$, where N is the number of turns. Therefore we conclude that the ideal helix cannot be unwound by $E \perp h$ without nucleation of defects due to thermal fluctuations or other non-homogeneities (for instance at anchoring boundaries).

3. Field induced anharmonicity

3.1 Spectra of the photonic stop-band

The optical transmission of non-polarised light has been calculated for the same distorted texture within the spectral range of the Bragg reflection (see Figure 5). The refraction indices were taken from the experiment, $n_{\|}$ = 1.550, $n_{\perp}$ = 1.474. With increasing field, the Bragg minimum shifts slightly to *shorter* wavelengths due to the helix distortion seen in Figure 4. Finally the stop-band completely disappears due to helix unwinding at a field of about 25 V μm^{-1}, which is much higher than the value predicted by Equation (6). In fact, the high-field simulated unwinding is caused by finite space sampling δz along the z-axis that is necessary for numerical calculations. When a size of the walls W (Figure 2(c)) becomes comparable with the discrete value of δz the calculation accuracy decreases, which results in an apparent 'untwisting' effect. Decreasing δz increases the unwinding field. In some sense, a finite value of δz numerically mimics a 'defect', which allows overcoming the mentioned topological constraints.

We have carried out a special experiment to check the results of our modelling. A chiral mixture of MLC6601 + 21.7% ZLI-811 (both from Merck) was used with P_0 = 0.42 μm ($\partial P_0/\partial T < 0$), $\varepsilon_a \approx 6$, $K_{22} \approx$ 6 pN, $n_{\|} \approx 1.55$, $n_{\perp} \approx 1.47$. The interdigitated electrodes (Figure 3) were covered with polyimide but not rubbed to reduce the azimuthal anchoring energy W_{a2} to a minimum. This should allow the director to rotate freely within the plane of the cell at the bottom interface. The top glass substrate was covered with polyimide and rubbed to provide good quality planar helical texture. The gap between glasses (d = 12 μm) was filled with the mixture in the isotropic phase. To avoid any thermal and hydrodynamic processes an optimum frequency of external field was chosen of 500 Hz, the voltage U(rms) being varied from 0 to 120 V.

Figure 6 shows the results of our experiment. As seen from the figure, with increasing field the Bragg minimum broadens and finally disappears. The field necessary for the complete disappearance of the Bragg reflection (about 6 V μm^{-1}) approximately corresponds to the estimated critical field $E_c = (\pi^2/P_0)(4\pi K/\varepsilon_a)^{1/2} \approx 7$ V μm^{-1}. However, no shift to longer wavelengths is seen, which would be indicative of helix

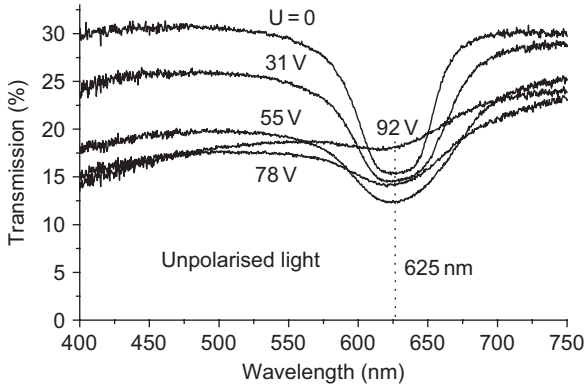

Figure 6. Experimental transmission spectra of the planar cholesteric texture as function of the external field (unpolarised light). The absolute value of the transmission is reduced by the system of non-transparent interdigitated electrodes. Note a small shift of the Bragg minimum to *shorter* wavelengths.

unwinding. On the contrary, there is a small shift to *shorter* wavelengths predicted by modelling. Under a microscope the field-induced grid of defects is seen at a voltage exceeding 70 V.

Our conclusion from both the experiment and the modelling is that, *in the absence of defects, the field cannot increase the period of the helix*. Therefore, the helix unwinding effect cannot be used for fast switching of the spectral position of the photonic stop-band, at least, over such a large wavelength range as follows from the expected ratio of $P/P_0 = 1.6$ (see Figure 1(b)). Indeed, it would open almost the whole visible range of λ = 400–600 nm for tuning lasers on cholesteric liquid crystals. In reality, we may only use the small shift of the long-wave edge of the photonic band to the longer wavelengths that is seen in Figure 5. It is also possible to use a small red shift of the band due to tuning the helical axis direction (*9*) or changing the shape of the photonic band for rather limited tuning of the wavelength of lasing (*10*). Fortunately, there is a possibility for designing multilayer cholesteric–nematic lasers, in which a function of electric field tuning of laser intensity and wavelength is transferred from a cholesteric to a nematic layer (*11*).

3.2 *Fourier transform of director distribution*

As seen in Figure 4, a sufficiently strong electric field perpendicular to the helical axis causes a snake-like distortion of the director field with the pitch of the helical structure remaining unchanged. The distribution of the *x*- and *y*-components of the director is no longer described by a simple sine law but contains a contribution of higher harmonics:

$$n_x(z) = A_{1,x}\sin(q_0 z) + \sum_m \left(A_{m,x}\sin(mq_0 z) + B_{m,x}\cos(mq_0 z)\right)$$
$$n_y(z) = A_{1,y}\sin(q_0 z) + \sum_m \left(A_{m,y}\sin(mq_0 z) + B_{m,y}\cos(mq_0 z)\right). \quad (8)$$

Due to the sine form of the initial distribution of the director and quadrupolar character of its coupling to the electric field, the odd harmonics will be dominating ($m = 2k + 1$, where k = 1, 2, 3, ...). The amplitudes of the harmonics characterise a degree of the field-induced anharmonicity of the helical structure.

We have made a simulation of the higher harmonics appearance and optical properties of the cholesteric structure with the following parameters typical of chiral materials based on the well-known nematic mixture E7: helical pitch 0.4 μm, elastic modulus K_{22} = 5 pN; principal dielectric permittivity values $\varepsilon_{\|} = 20$, $\varepsilon_{\perp} = 8$; refraction indices $n_{\|} = 1.7$, $n_{\perp}$=1.5. Cell thickness is d = 10 μm, zenithal and azimuthal anchoring energies is strong ($W_{z,a}$ = 0.1 mJ m^{-2}) at both boundaries. The electric voltage is applied across the in-plane electrodes separated by a distance of l = 20 μm (see Figure 3). The helix is confined by two glasses with refractive index n_g = 1.5.

The inset in Figure 7 shows the calculated space dependence of the *x*-component of the director $n_x(z)$ within one period of the cholesteric structure. The

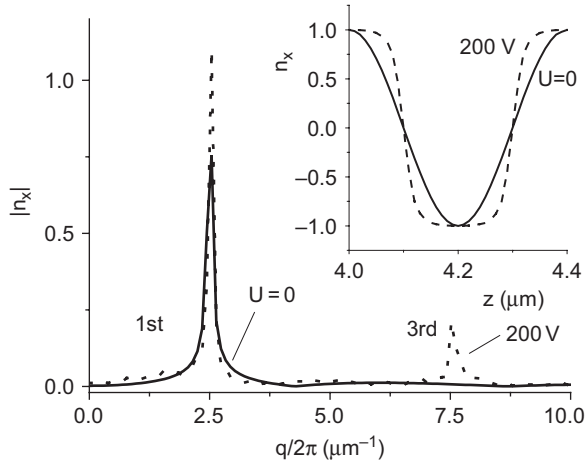

Figure 7. Inset: calculated space dependence of the *x*-component of the director $n_x(z)$ within one period of the cholesteric structure with P_0 = 0.4 μm. Main plot: Fourier transform $n_x(q)$ showing appearance of the third harmonic of the helix in a strong field. In both plots solid lines correspond to zero voltage, dot (or dash) curves for U = 200 V. For parameters see the text.

voltage applied to the in-plane electrodes is either 0 or 200 V (E = 10 V μm^{-1}). As expected, at the field applied, the apices of the curve $n_x(z)$ for U = 200 V become very flat. The main plot of Figure 7 represents the Fourier transform of $n_x(q/2\pi)$. In the field absence, on the wave vector axis, the helix is represented by a single harmonic at $q/2\pi = q_0/2\pi = 1/P_0 = 2.5\ \mu m^{-1}$. At a high voltage, a strong third harmonic of the distorted helix appears at $q/2\pi = 3q_0/2\pi = 3P_0 = 7.5\ \mu m^{-1}$. The amplitude of the third harmonic reaches a value as high as 27% of the first harmonic amplitude at zero field. Note that the characteristic relaxation time of any elastic distortion mode is described by the universal formula $\tau = \gamma/Kq^2$, where γ is a rotational viscosity. Therefore the third harmonic of the distortion should relax nine times faster than a distortion on the helix pitch scale. This fact is of *principal importance* for the fast devices based on the helix anharmonicity.

3.3 Second order photonic band

The helix distortion influences the optical properties of the helical structure; in particular, the field should induce higher harmonics in the transmission and reflection spectra. This phenomenon had been observed long ago with the help of the electro-transmission technique (*9*), but only recently did we understand that it might be very interesting for application to photonics. Indeed, with an experimental cell of the type shown in Figure 3, one can observe several spectacular effects. For example, if the cholesteric is doped with a luminescent dye and the dye is pumped by a light within the dye absorption band, one can observe a light amplification or lasing effect not only at the edge of the photonic band but at other frequencies as well. To this effect, the pump energy should be sufficient to create the inverse electron population between the two appropriate (lasing) levels.

First, we calculated the field-induced transmission spectra without amplification (in the so-called cold regime). They are shown in Figure 8. For calculations, it was assumed that a circularly-polarised, slightly incoherent probe beam impinges on the helix along its axis. The latter allows escaping a Fabri–Perot effect caused by thick glass substrates confining the cholesteric layer. In zero field, the cold structure shows a typical Bragg reflection (photonic stop-band), Figure 8(a), centred at $\lambda_1 \approx 640$ nm with no trace of higher orders. With increasing field, Figure 8(b,c), a new structure (an explanation is given below) appears within the Bragg band and a sharp minimum develops corresponding to the second order reflection at 320 nm. The transmission is almost completely suppressed within a narrow spectral band centred at $\lambda_2 \approx 320$ nm. It means that all of the light of the probe beam within this narrow band is reflected.

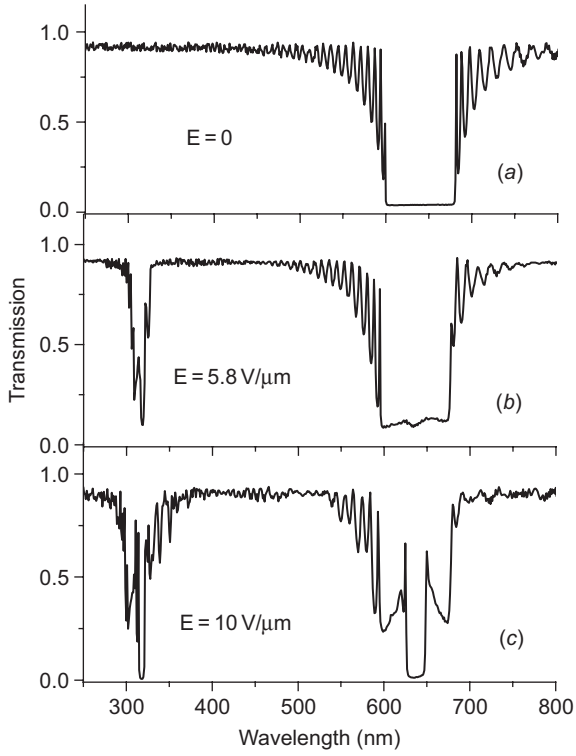

Figure 8. Calculated transmission spectra of the first and second order photonic bands for three values of the applied field shown in the figures (absorption coefficient $\alpha = 0$).

The appearance of the 'second order' reflection in the spectrum is a fingerprint of the field-induced third harmonic in the cholesteric helix shown in the Fourier spectrum (Figure 7). It can be understood in terms of the scattering amplitude approach discussed by de Gennes and Prost (*12*). The light scattering amplitudes are proportional to Fourier components of the dielectric tensor $\varepsilon(q)$, where now $q = k_0 - k_1$ is the scattering wavevector. All three vectors q, k_0 (for incident wave) and k_1 (for reflected wave) are parallel to the helix axis z and $q_0 > 0$ means the right-handed helix. The components of the local dielectric permittivity tensor are as follows:

$$\varepsilon_{ij} = \varepsilon_\perp \delta_{i,j} + \varepsilon_a\, n_i\, n_j, \tag{9}$$

where n_i are director components with $i,j \in \{1,2,3\}$. Following de Gennes and Prost we restrict our analysis to considering only a single (ε_{xx}) component of the dielectric tensor.

For the cholesteric helix distorted by an electric field applied along the x-axis, the z-dependence of the ε_{xx} component with allowance for the field-induced third harmonic in the director distribution can be written as:

$$\varepsilon_{xx}(z) = \varepsilon_\perp + \varepsilon_a n_x^2(z) = \varepsilon_\perp + \varepsilon_a(A_1\cos(q_0 z) + A_3\cos(3q_0 z + \varphi_0))^2, \quad (10)$$

where φ_0 is a phase shift between the third and first harmonics. From the condition $n_x = 0$ at $q_0 z = \pi/2 + k\pi$ (here k is an integer number) for both non-distorted and distorted helix, we find $\varphi_0 = 0$. Thus for the Fourier component ε_{xx} we have:

$$\begin{aligned}\varepsilon_{xx}(q) &= \int_z \varepsilon_{xx}(z)e^{iqz}dz \\ &= \varepsilon_a \int_z (A_1\cos(q_0 z) + A_3\cos(3q_0 z))^2 e^{iqz}dz = \\ &= \varepsilon_a\left[\frac{A_1^2}{4} + \frac{A_1 A_3}{2}\right]\int_z \left(e^{i(2q_0+q)z} + e^{i(q-2q_0)z}\right)dz \\ &\quad + \varepsilon_a \frac{A_1 A_3}{2}\int_z \left(e^{i(q+4q_0)z} + e^{i(q-4q_0)z}\right)dz \\ &\quad + \varepsilon_a \frac{A_3^2}{4}\int_z \left(e^{i(q+6q_0)z} + e^{i(q-6q_0)z}\right)dz. \end{aligned} \quad (11)$$

Equation (11) shows that the integral is not zero only if $q = \pm 2q_0$, $q = \pm 4q_0$ and $q = \pm 6q_0$.

Restricting ourselves to linear optics when frequencies of the reflected and incident waves are equal, we take solutions for which the incident and reflected light have wave vectors of opposite signs ($k_1 = -k_0$). The latter gives an additional selection rule and results in scattering vectors limited to a set of positive values: $q = +2q_0$, $q = +4q_0$ and $q = +6q_0$. The negative scattering vectors are excluded, due to the equality of frequencies mentioned. As $q = k_0 - k_1$ and $k_1 = -k_0$, from a set of scattering vectors $q = +2q_0$, $q = +4q_0$ and $q = +6q_0$ we get three frequency bands corresponding to incident light wave vectors: $k_0 = q_0$, $k_0 = 2q_0$ and $k_0 = 3q_0$. We use term 'frequency bands' because, in cholesteric media, the local refractive index is varied from $n_\perp$ to $n_\parallel$ and there are many frequencies ω within $ck_0/n_\parallel$ and $ck_0/n_\perp$, where c is light velocity in vacuum, corresponding to wave vector k_0.

It is important to mention that if $A_3 = 0$ (non-distorted helix) then only the first optical band ($k_0 = q_0$) is allowed, which is centred at a vacuum wavelength $\lambda = 2\pi\langle n\rangle/q_0 \equiv \langle n\rangle P_0$, where $\langle n\rangle$ is an average refractive index. The presence of the third harmonic ($A_3 \neq 0$) in the director field distributions allows for the second ($k_0 = 2q_0$, $\lambda = \langle n\rangle P_0/2$) and third ($k_0 = 3q_0$, $\lambda = \langle n\rangle P_0/3$) bands centred at the double and triple optical frequency respectively. The second photonic band (at $\lambda = 320$ nm) is a result of optical mixing of the first and second harmonics in the distorted helix. This mixing is a consequence of the non-linear relation (Equation (9)) between the dielectric tensor components and the director field distribution. Moreover, according to the first integral at the right side of Equation (11), the mixing effect also influences the principal photonic band by the appearance of the pronounced minimum in the transmission seen well in Figure 8(c) at $\lambda = 640$ nm.

3.4 Lasing

We have also calculated the field-induced lasing spectra for an amplifying (with negative absorption or gain) cholesteric layer. Locally, the gain is introduced as a positive gain index α in an exponentially increasing function $\exp(\alpha x)$ with distance x exactly as the absorption coefficient k enters the Buger law $\exp(-kx)$ for a uniform medium.

Figure 9 shows the *amplified* transmission spectra (AT) near both the first and second order Bragg bands calculated for a cholesteric having gain coefficients ($\alpha_\parallel = 0.2\ \mu m^{-1}$, $\alpha_\perp = 0$). At zero field (Figure 9(a)), the helix is undistorted and we observe multimode lasing at the long-wave edge of the first order Bragg band (a single mode laser generation can be obtained at a lower gain coefficient of the order of $\alpha \approx 0.01\ \mu m^{-1}$.

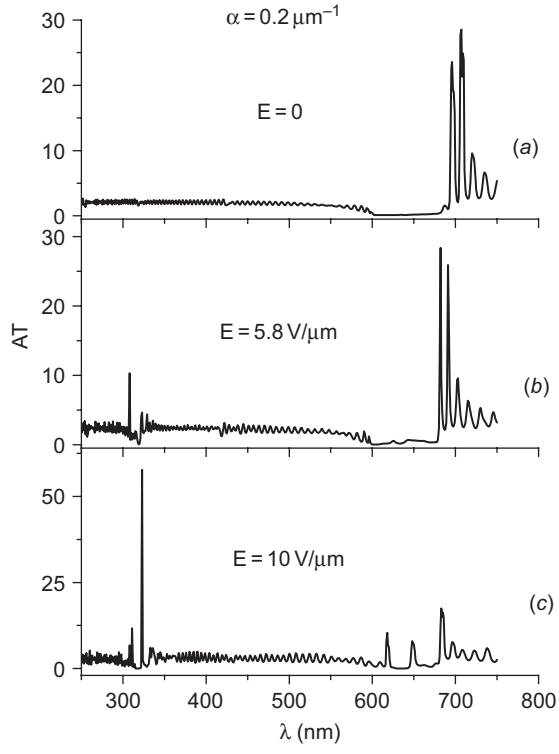

Figure 9. Calculated amplified transmission spectra of the first and second order photonic bands for three values of the applied field (gain coefficient $\alpha = 0.2\ \mu m^{-1}$).

No trace of lasing is seen at $\lambda_2 \approx 320$ nm. With increasing field, at a certain critical value of $E_c \approx 5.5$ V μm^{-1} the lasing appears at the second order photonic band (Figure 9(b)). At a higher field a sharp lasing line is seen at the long-wave edge of the second order band (Figure 9(c)). It could be a single mode lasing if the spectral range of the negative absorption were limited to the wavelengths of, say, 320–340 nm. As to the experiment, it can be done using any standard laser (e.g. N_2 laser) as a pump source, a laser dye absorbing the pump energy and a cholesteric liquid crystal with a helical pitch tuned so that the second order band would coincide with the dye luminescent band.

It may seem that an electric field of about 10 V μm^{-1} necessary for this sort of experiment is too high. Indeed, according to the de Gennes formula (Equation (6)), the helix is unwound at about $E_c \approx 7$ V μm^{-1}. However, we should not forget that in the absence of defects, the cholesteric–nematic transition would not occur at all. In a more realistic situation, some defects are always present, but the process of helix unwinding is very slow (seconds or minutes). To our experience, at low repetition frequency ~10 Hz and duration of electric field pulses less than 1 ms, one can escape defects nucleation, and the helix is still twisted even at a field strength a few times higher than the critical field discussed above. Therefore, for the strong helix distortion and observation of the laser effect on the second order stop-band, one has to use sub-millisecond field pulses synchronised with optical pumping pulses. Note that the breakdown voltage also increases with pulse shortening.

4. Electro-optics of the distorted helix

4.1 The principle

The director orientation effects in liquid crystals, due to anisotropy of dielectric and optical properties of the latter, can be used for the control of light polarisation by an electric field. In particular, the electro-optical in-plane switching (IPS) mode is widely used in displays based on nematic and cholesteric liquid crystals (CLC) manifesting texture transitions (*13*, *14*). In both cases, the switching times were not short enough. We suggest using field-induced anharmonicity of the cholesteric helix to reduce considerably the device response time in IPS mode.

Figure 10 shows an example of the simulated evolution of the light polarisation states at an output of

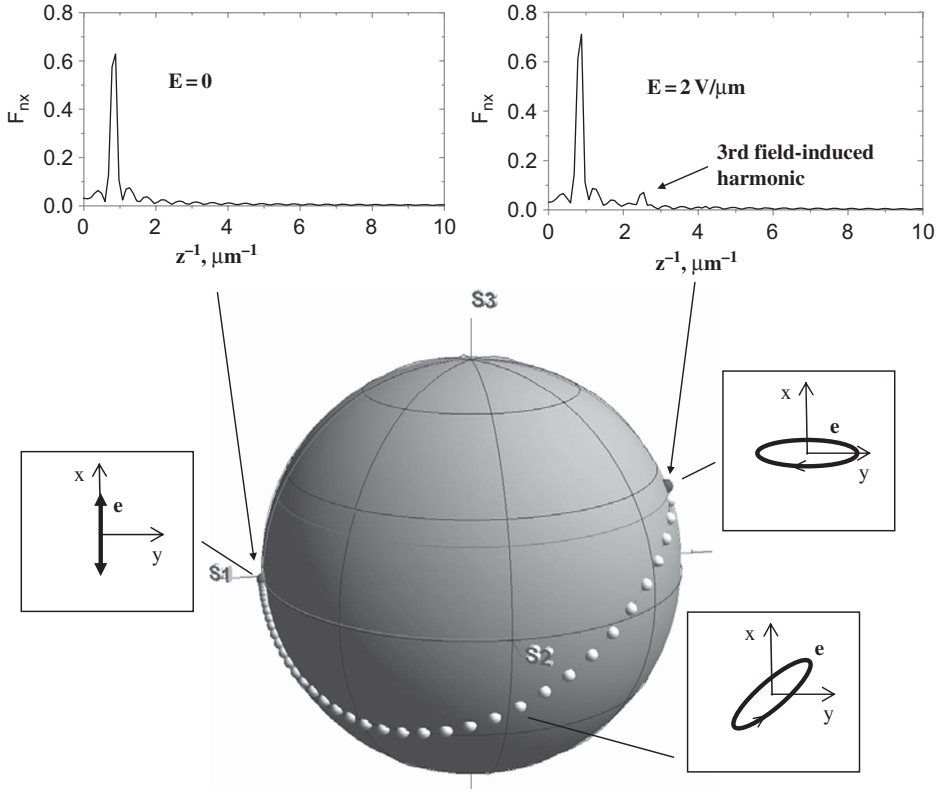

Figure 10. Poincare sphere presentation of light polarisation states at the output of a cholesteric liquid crystal layer upon increasing the in-plane electric field from 0 to 2 V μm^{-1} with a step of 0.05 V μm^{-1}. Top insets show Fourier spectra of n_x director component at zero and maximum electric field.

the cholesteric layer subjected to the in-plane electric field along the x-axis. In this particular case, the helix pitch and thickness of the layer are 1.2 μm and 8 μm respectively. The calculations are done for a wavelength of 550 nm. Typical values of CLC parameters used are: dielectric anisotropy $\varepsilon_\alpha = 15$, optical anisotropy $\Delta n = 0.2$, twist elastic constant $K_{22} = 5$ pN. Here, an important issue is that even a small degree of the induced anharmonicity (amplitude of induced third harmonic is about 5% of the fundamental one; see inset in Figure 10) results in dramatic changes in the polarisation of the light transmitted by a cholesteric layer. Increasing field from 0 to 2 V μm^{-1} covers a continuous range of light polarisation states between the two orthogonal polarisations represented by opposite points on the Poincare sphere (Figure 10). It is the essence of the new effect and the display based on the latter (*15*).

According to data in Figure 10 the field-off polarisation state is linearly polarised (located at the equator on the Poincare sphere), so it can be completely blocked by a properly oriented analyser placed at the output of the layer. However, it is also important to mention that, to achieve the proper linear polarisation at the output, the linear polarisation at the input of the layer should also be properly adjusted. In the given example, in order to get the field-off state linearly polarised along the x-axis, the light at the input should be linearly polarised at an angle of –60° with respect to the same x-axis. It means that a very high contrast determined solely by the quality of polarisers can be achieved at a particular wavelength, when the angular positions of a polariser and an analyser are tuned separately and very precisely. The second useful property has been mentioned above: the relaxation time of high harmonics of the helix is inversely proportional to the square of the harmonic number, $\tau_m \propto m^{-2}$. Therefore, a fast, high-contrast light modulator can be designed on the anharmonicity effect.

4.2 *Modelling and experiment*

For a study of the dynamics of the electro-optical effect we use the same basic geometry of Figure 3. However, now the helical pitch is larger ($P_0 > 1$ μm) and the Bragg stop-band is in the infrared range ($\lambda_{B1} = <n>P_0$). The light of a He-Ne laser ($\lambda = 633$ nm) is transmitted through the cell along the helical axis, the cell being placed between a polariser and an analyser. Figure 11 shows the result of our modelling for the following cell parameters: thickness $d = 7.5\mu$m, gap between electrodes 20 μm, voltage $U = 20$ V, rubbing direction at 45° to the electrode stripes, material rotational viscosity 0.2 Pa·s, dielectric and optical anisotropy $\varepsilon_a = 12.1$, $\Delta n = 0.19$.

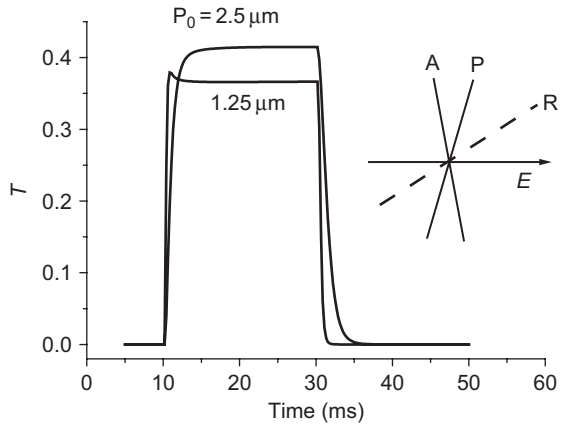

Figure 11. Calculated optical response (absolute value of transmission at $\lambda = 633$ nm) of two cholesteric cells to the voltage pulse in the in-plane switching mode. Equilibrium pitches are 2.5 and 1.25 μm for the two cells. Correspondingly, the applied voltages are 20 and 35 V. Inset: angular directions of rubbing (R), polariser (P) and analyser (A) with respect to the electric field E.

Our modelling shows that for each particular set of the cell parameters there exists a unique, 'magic' combination of the angular positions of polariser and analyser, for which, at zero field, the outgoing light is completely blocked. At the same time, a reasonable field results in a high transmission (T) determined solely by the analyser. For instance, for the helical pitch of 2.5 μm the angles of the polariser and analyser are $\varphi_1 = 83°$ and $\varphi_2 = 97°$ with respect to the field direction (see inset in Figure 11) and we obtain $T = 0.35 – 0.4$ and contrast ratio $K \approx 1000{:}1$ ($\lambda = 633$ nm, $E = 1$ V μm^{-1}). Corresponding switch-on and switch-off times taken by convention between 10% and 90% of the maximum transmission T are $\tau_{on} = \tau_{off} \approx 2.3$ ms. For exponential function $e^{-t/\tau}$, the characteristic time is 2.2 times less: $\tau \approx 1$ ms. For $P_0 = 1.25$ μm the contrast is almost the same (with $\varphi_1 = 65°$ and $\varphi_2 = 114°$ and $E = 1.75$ V μm^{-1}) and switching times are shorter, $\tau_{on} \approx \tau_{off} \approx 0.5$ ms ($T = 10$–90%). The corresponding characteristic time is $\tau \approx 0.23$ ms.

From the analytic formula for the elastic relaxation time of different harmonics with number m,

$$\tau_m = \frac{\gamma}{K_{22} m^2 q_0^2}, \qquad (12)$$

we find $\tau(m = 1,2,3) = 1.58$, 0.395 and 0.175 ms, respectively (for $P_0 = 1.25$ μm and the same γ and K_{22} used in modelling). We can see that the time found from modelling (0.23 ms) is close to the relaxation time of the third harmonic (0.175 ms). Such a difference is expected because the first harmonic of the helix was also influenced by the field (it is increasing; see

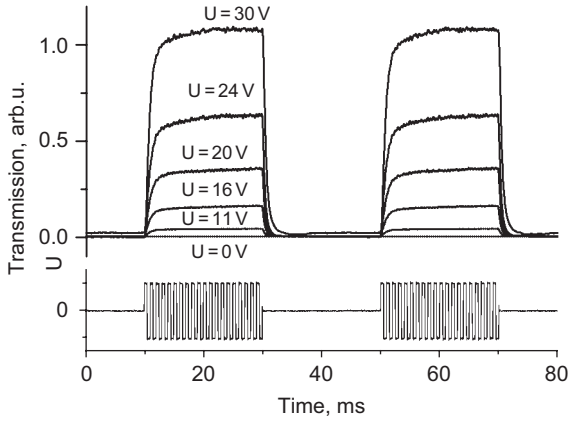

Figure 12. Experimental oscillograms of the cell optical response (top) to voltage pulses of variable amplitude (bottom). For parameters see the text.

Figure 7) and should participate in the overall switching process with a larger time $\tau(m = 1) = 1.58$ ms. For cholesteric with $P_0 = 2.5$ μm, according to Equation (12), the switching time should be four times longer than for $P_0 = 1.25$ μm; indeed, the ratio 2.3/0.5 = 4.6 is close to the expected value.

The experimental results shown in Figure 12 agree with the principal predictions of the simulation. The experiment is made with the substance and cell parameters close to that used in modelling: $P_0 = 1.2$ μm, ε_a = 12.1 (at $f = 1$ kHz), optical anisotropy $\Delta n = 0.19$, (at λ = 589 nm), twist elastic coefficient $K_{22} \approx 5$ pN, twist viscosity 0.2 Pa·s. With $U = 20$ V, $\varphi_1 = 39°$ and φ_2 = 110° we obtain a contrast of 140:1, and switching times τ_{on} = 1.8 ms, τ_{off} = 0.9 ms (*15*). The switching-off characteristic time $\tau = 0.9/2.2 = 0.4$ ms is much shorter than the relaxation time of the first harmonic (1.58 ms) but 1.7 times longer than our simulation result (0.23 ms). As to τ_{on}, it is twice as large as τ_{off}. This asymmetry is not yet understood; it could be related to field inhomogeneity, insufficiently strong anchoring energy, or the presence of some defects. Nevertheless, the switching times are sufficiently short, for low-field ($E \approx 1$ V μm^{-1}) high-contrast liquid crystal modulators and shutters. For shorter pitch materials we expect switching time to be even less than 100 μs.

5. Conclusion

In conclusion, we have discussed optical and electro-optical properties of the defect-free cholesteric in the electric field strictly perpendicular to the helical axis. This is an almost ideal case, which, however, can be realised in practice. In thermodynamic equilibrium, as is well known from the classical de Gennes work, the electric field distorted helix has higher free energy in comparison with the unwound helix. However, our simulation and experimental work presented here proves that, in the absence of defects, the helix cannot be unwound for topological reasons. Instead, the field deforms the helix without a change of its period and induces high harmonics of the helical structure. It has been shown that, due to the appearance of higher harmonics, the shape of the photonic stop-band changes and the second-order photonic band appears in the optical transmission. We have also predicted a laser effect on the second order photonic band in a distorted cholesteric with negative absorption. Next, our modelling shows that the field-induced anharmonicity results in a strong change of the polarisation state of the light beam passing the helical structure along its axis. Because the field induces only the odd harmonics in the helical structure they relax much faster than the first (fundamental) one. It is proved by the IPS experiments that the switching times of the devices using the corresponding electro-optical effect are reduced significantly.

Acknowledgements

The authors are grateful to their colleagues Dr. M.I. Barnik, Dr. B.A. Umanskii and Dr. N.M. Shtykov for many useful discussions related to the problem. The work is supported in the frame of Basic Research Programs of Physical Sciences Department of Russian Academy of Sciences.

References

(1) de Gennes, P.G. (a) *Sol. State. Commun*. **1968**, *6*, 163; (b) *C. R. Acad. Sci*. **1968,** *B266*, 15; (c) *J. Chem. Phys*. **1969,** *51*, 816; (d) *Phys. Lett*. **1969,** *30A*, 454; (e) *J. Phys. (Paris)* **1969,** *30* (Colloq. C4), C4-65.
(2) Meyer, R.B. *Appl. Phys. Lett*. **1969**, *14*, 208.
(3) Kawachi, M.; Kogure, O. *Jap. J. Appl. Phys*. **1977**, *16*, 1673.
(4) Durand, G.; Leger, L.; Rondelez, F.; Veyssie, M. *Phys. Rev. Lett*. **1969**, *22*, 227.
(5) Palto, S.P. *Zh. Eksp. Teor. Fiz*. **2002**, *121*, 1; *JETP*, **2002,** *94*, 260.
(6) Palto, S.P.; Blinov, L.M. *J. Soc. Elect. Mat*. Eng. **2005**, *14*, 115.
(7) Palto, S.P. *Zh. Eksp. Teor. Fiz.* **2001**, *119*, 638; *JETP* **2001,** *92*, 552.
(8) Palto, S.P. *Kristallografia* **2003**, *48*, 130; *Crystallography Reports* **2003,** *48*, 124.
(9) Blinov, L.M.; Belyayev, S.V.; Kizel', V.A. *Phys. Lett*. **1978**, *65A*, 33; *Pis'ma Zh. Eksp. Teor. Fiz.* **1979,** *29*, 344.
(10) Yu, H.; Tang, B.Y.; Li, J.; Li, L. *Opt. Express.* **2005**, *13*, 7243.
(11) Barnik, M.I.; Blinov, L.M.; Lazarev, V.V.; Palto, S.P.; Umanskii, B.A.; Shtykov, N.M. *J. Appl. Phys.* **2008**, *103*, 123113.
(12) de Gennes, P.G.; Prost, J. *The Physics of Liquid Crystals*; Clarendon Press: Oxford, 1993.

(13) Blinov, L.M.; Chigrinov, V.G. *Electrooptic Effects in Liquid Crystals Materials*; Springer-Verlag: New York, **1994**.
(14) Lueder, E. *Liquid Crystal Displays*; John Wiley & Sons: Chichester, **2001**; p.116.
(15) Barnik, M.I.; Blinov, L.M.; Palto, S.P.; Shtykov, N.M.; Umanskii, B.A. *Fast In-plane Switching Mode in Cholesteric Liquid Crystals*, Proceedings of the 27th International Display Research Conference, SID Eurodisplay **2007**, s. 5-4, pp. 97–100.